XLI CILAMCE
XLI Ibero-Latin American Congress on Computational Methods in Engineering
16-19 November, 2020 FOZ DO IGUAÇU PARANÁ - BRAZIL

DNS of a small roughness immersed in a boundary layer: body-fitted and approximated methods comparison

Fernando H. T. Himeno[1], Marlon S. Mathias[1], Marcello A. F. de Medeiros[1]

[1]*Department of Aeronautical Engineering, University of Sao Paulo*
Av. Joao Dagnone, 1100, 13563-120, Sao Paulo/Sao Carlos, Brazil
fernando.himeno@usp.br, marlon.sproesser@usp.br, marcello@sc.usp.br

Abstract. The laminar to turbulent flow transition often initiates from small and irregular disturbances which interact with boundary layers. At some specific amplitude and frequency band, these disturbances generate Tollmien-Schlichting (T-S) waves which may evolve leading to turbulence in such a process that is very sensitive to the surface smoothness. Account the effect of tiny roughnesses commonly represent a great difficulty to experimental and numerical studies. Here we present some of these limitations observed on simulating a rectangular and localized small roughness placed on zero-gradient flat plate. This study is conducted using a compressible DNS code at a low Mach regime. We also compare the numerical results obtained by two approaches used for modeling such a small roughness: a) meshing the element and applying immersed walls conditions and b) approximating the roughness effect by a non-homogeneous condition on the plate surface at roughness location. Preliminary results from bidimensional simulations shows that the second approach, b), might present a small phase shift and low amplitude mismatch when compared to the meshed element. In contrast, we also observe the higher cost on simulating tiny roughnesses with immersed walls.

Keywords: Boundary Layer Transition, DNS, Roughness.

1 Introduction

In the context of fluid dynamics and aeronautical applications, a reasonable prediction of the friction drag relies on a good representation of the boundary layer formed around its surfaces. It is known that the turbulent boundary layer flow is characterized by drag increase relative to the laminar one. Hence, for an aircraft, the greater the region with turbulent flow, the greater the fuel consumption and, consequently, the lower its payload. For a commercial aircraft, for example, it is estimated that 50% of the total drag is due to its friction component and 25% of this number is a contribution from wings surfaces [1].

The understanding of the laminar-turbulent transition phenomena means accurate prediction of the aircraft drag. The transition process, however, is very complex and differs considerably from the known contained flows and free shear layer problems, since it is sensitive not only to the inherent boundary layer characteristics but also to external disturbances such as free-stream turbulence, acoustic noise and surface irregularities [2, 3]. In the initial stages of the smooth transition process these external disturbances penetrates the boundary layer on a mechanism known as receptivity [2]. Depending on the amplitude and frequency of these perturbations, they evolve generating the known Tollmien-Schlichting (T-S) waves which eventually increase in amplitude and further leads to transition as they convect downstream.

On this scenario, the present study aims at numerically investigate the effects which a small roughness placed over a flat plate has in the boundary layer which could eventually lead to transition. Here, the T-S wave is artificially imposed at plate wall upstream to the roughness location which is not usually considered in the small roughness studies that are mainly interested on the T-S waves generated by the presence of roughness itself not by a prior T-S. This scenario was studied experimentally by [4] which parameters was used to determine the present numerical simulations setup.

Investigate the effects of a very small excrescence is a difficult task for both experiments and simulations due to the dimensions of this element. In numerical studies, meshing such a small element requires high refinement which increases computational cost. Moreover, for many used codes it can be even impossible to set the refinement needed to include roughness with heights in the order of 1% of the boundary layer thickness [5]. Hence, a common

approach to circumvent this problem is made by an approximation of the roughness element by a non-homogeneous boundary condition on the plate wall that mimics its local effect. The values for this method are obtained via a Taylor expansion of the flow profile without any roughness in which a linear behavior of this profile is assumed for a very small element. This has been successfully applied in the context of receptivity to acoustic waves [6–10]. This method presents a good agreement compared to body fitted up to roughness heights around 10% of the displacement thickness [5], which is the order of the roughness height of the elements simulated in this work.

Differently from receptivity studies, here we consider the interaction a prior T-S wave generated upstream to the roughness element. For modeling this small element, the body-fitted and Taylor expansion approaches are compared. We are most interested in the validation of the approximated one which presents low computational cost compared to the meshed element.

2 Numerical methods and simulation setup

2.1 DNS code

This study is conducted using a Direct Numerical Simulation (DNS) code which directly solves the set of equations composed by the Navier-Stokes (compressible and non-conservative form), mass and energy conservation equations,

$$\frac{\partial u_j}{\partial t} = -\frac{\partial u_j}{\partial x_i}u_i - \frac{1}{\rho}\frac{\partial p}{\partial x_j} + \frac{1}{\rho}\frac{\partial \tau_{ij}}{\partial x_i}, \tag{1}$$

$$\frac{\partial \rho}{\partial t} = -\rho\frac{\partial u_i}{\partial x_i} - \frac{\partial \rho}{\partial x_i}u_i, \tag{2}$$

$$\frac{\partial e}{\partial t} = -\frac{\partial e}{\partial x_i}u_i - \frac{p}{\rho}\frac{\partial u_i}{\partial x_i} + \frac{1}{\rho}\tau_{ij}\frac{\partial u_j}{\partial x_i} - \frac{1}{\rho}\frac{\partial q_i}{\partial x_i}, \tag{3}$$

where u_i represent the velocities components, ρ, density, p, pressure, e, energy and x_i, the axis vectors. τ and q are the viscous tensor and heat flux, respectively. The variables are non-dimensionalized by the boundary layer displacement thickness at a reference location on the plate, δ_0^*, and also by the free-stream velocity and density, U_∞^* and ρ_∞^*.

Mesh is cartesian and allows the refinement of the most critical regions as the plate leading edge and disturbances locations. The time integration is done by a 4th order Runge-Kutta scheme. The derivatives are calculated using a spectral finite difference scheme of 6th order, based on method presented by [11].

Figure 1 shows a scheme of the simulation domain and also summarizes some of the boundary conditions applied which includes the meshed rectangular roughness element modeled as a immersed wall.

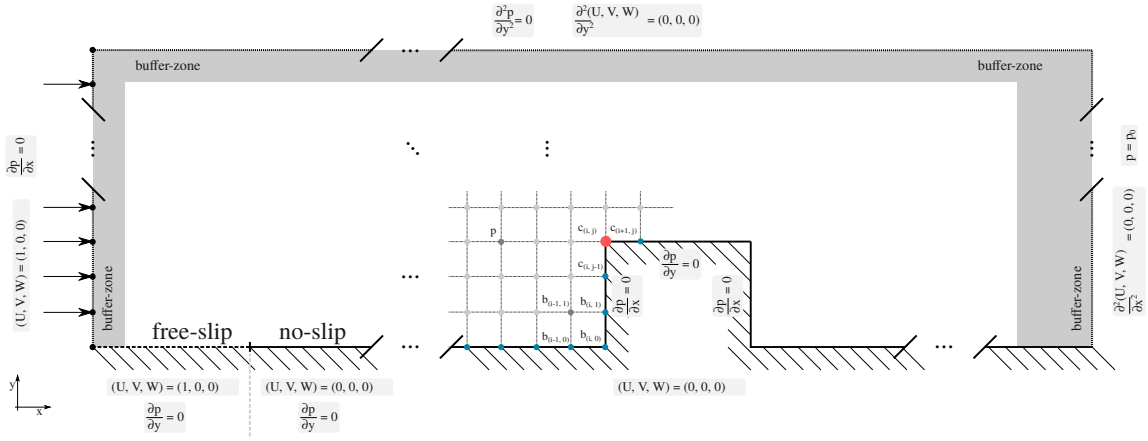

Figure 1. Computational domain scheme and boundary conditions.

The code is implemented in *Fortran 90* and parallelized via *MPI* (*Message Passage Interface*) and OpenMP (*Open Multi-Processing*). The domain is decomposed by 2DECOMP&FFT library [12]. Further details of the DNS code implementation are presented in some previous publications of the present group [13–18].

The small roughness approximation approach assumes that its immersed walls effects can be transferred to the plate wall as a non-homogeneous condition. The values of this slip condition are obtained via Taylor expansion applied in velocities profiles,

$$u_T(x) = -h_R \left.\frac{\partial u(x,y)}{\partial y}\right|_{y=0} + \frac{{h_R}^2}{2} \left.\frac{\partial^2 u(x,y)}{\partial y^2}\right|_{y=0}, \tag{4}$$

$$v_T(x) = -h_R \left.\frac{\partial v(x,y)}{\partial y(x,y)}\right|_{y=0} + \frac{{h_R}^2}{2} \left.\frac{\partial^2 v(x,y)}{\partial y^2}\right|_{y=0}. \tag{5}$$

In eq. (4) and eq. (5), a second order expansion is presented but the first order is usually enough. The Blasius boundary layer profiles can also be assumed in this method which avoids the need of a previous converged baseflow. In this work, however, it is consider the second order expansion and also a converged baseflow without any element as input for method.

2.2 Numerical setup

Parameters of simulations are chosen to reproduce the conditions of the experiments from [4] which studied a monochromatic T-S wave introduced upstream to the roughness. This experiment was conducted over an airfoil, but experiment conditions were set to obtain the maximum region with zero-gradient pressure along its surface. Then, along this region the Blasius boundary layer can be assumed and the simulations must have the same boundary layer parameters. Then, at the T-S disturbance and roughness locations, the Reynolds number based on the boundary layer displacement thickness (δ^*) are set to $Re_{\delta^*_D} = U_\infty \times \delta^*_D/\nu = 700$ and $Re_{\delta^*_R} = 950$, respectively, where ν is the kinematic viscosity.

The dimensional displacement thickness of $\delta^*_R = 0.55\ mm$ at the roughness location is considered as the reference length for non-dimensionalization of code parameters. The free-stream velocity used for the same procedure is the external boundary layer velocity from experiment, $U_0 = 27.5\ m/s$. The Mach number is fixed to $M = 0.3$ which are assumed to correspond to a condition closer enough to the incompressible flow condition with relative gains in simulation time.

Since the experiments used a cylindrical roughness with diameter equals to $10\ mm$ and simulations are conducted to a squared element, its dimensions are chosen to match a squared roughness circunscripted by the experiment cylinder. Then, the simulated roughness has a length of $\Delta L_R = 12.86$ ($7.07\ mm$). The simulated cases considers the roughness heights of $h_R = 0.05$ and 0.10 based on δ^*_R.

The physical domain in streamwise and perpendicular directions are defined as $-50 \leq x \leq 520$ ($-27.5 \leq x \leq 286.0\ mm$) and $0 \leq y \leq 16$ ($0 \leq y \leq 8.8\ mm$). For this domain, the total grid points are $n_x = 500$ and $n_y = 141$. The buffer-zones regions were composed by 20 and 60 points at the inflow and outer flow regions in streamwise direction, and 10 points at the open boundary region in the perpendicular direction. Figure 2 shows some details of this mesh and its grid stretching.

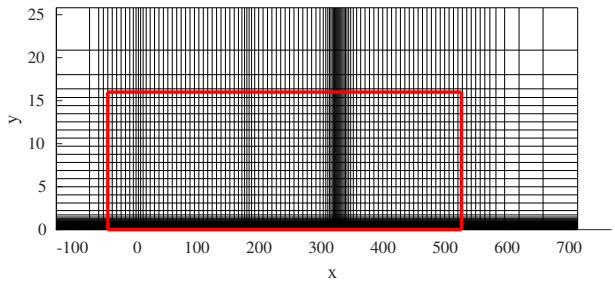

Figure 2. Mesh every 7 and 3 points in the x and y directions. The physical domain is showed delimited by the red lines.

Based on eq. (4) and eq. (5), the boundary conditions imposed at walls to approximate the meshed roughness of heights $h_R = 0.05$ and $0.10 \times \delta^*_R$ are showed by Fig. 3. Both calculated using a second order Taylor expansion of the velocity profiles obtained from a converged baseflow without any roughness.

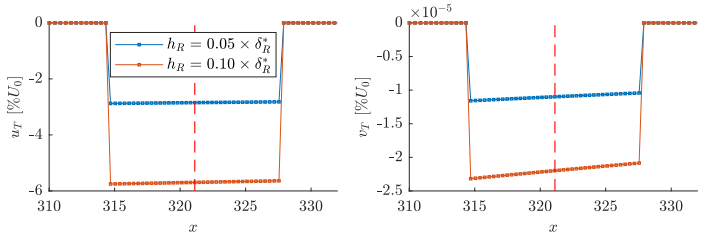

Figure 3. Boundary condition calculated via Taylor expansion approach imposed at plate wall to mimics the roughness effect.

3 Preliminary results and conclusions

Some preliminary results for the meanflow obtained from both methodologies are presented in Fig. 4 and Fig. 5, showing the streamlines and velocities contour fields. The approximation method seems to well represent the general behavior of the roughness nearfield distortions compared to the body-fitted approach. The most noticeable difference is observed mainly at the roughness corners which approximation method could not capture the abrupt velocity change. This pattern is clearer for higher roughness as expected since the assumption of small roughness is not as much valid as for the smaller one.

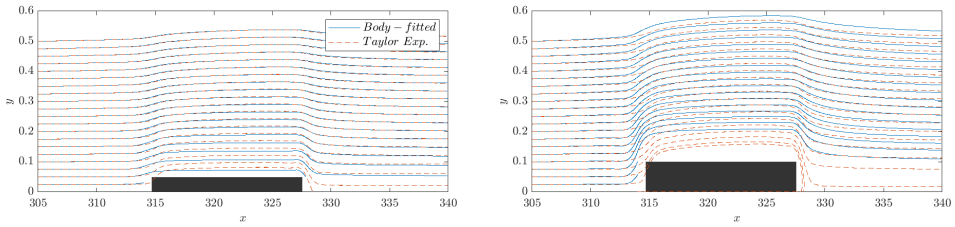

(a) $h_R = 0.05 \times \delta_R^*$ (b) $h_R = 0.10 \times \delta_R^*$

Figure 4. Baseflow streamlines comparing both roughness modelling approaches: *Body-fitted* and Taylor expansion.

For better compare both methodologies, a disturbance composed by a sum of T-S waves (wave packet), is imposed upstream to the roughness, centered at $x_D = 174.85$ ($Re_{\delta_D^*} = 700$) and spanning a length of $\Delta x_D = 19.5$. It is applied as a non-zero vertical velocity at the wall and composed by $N = 11$ modes of the fundamental frequency of $\omega_0 = 1.425 \times 10^{-2}$. This frequency band has a central frequency which corresponds to $\omega = 8.55 \times 10^{-2}$ ($F = (2\pi f\nu)/U_0^2 = 90 \times 10^{-6}$), the lower frequency used by the monochromatic disturbance from experiments [4]. A gaussian function with minimal amplitude of 1% of its maximum at $t = T_0/2$, is also applied along the disturbance packet on time for a smooth transition of the amplitude. Then, the disturbance function resumes as follows,

$$v(x,t)|_{y=0} = A_0\, F_x(x)\, F_t(t) \sum_{n=1}^{N} e^{in\omega_0(t-0.5T_0)}, \tag{6}$$

$$F_x(x) = e^{-\frac{(x-x_D)^2}{5}} - 0.5\, e^{-\frac{(x-x_D-\Delta x_D/5.16)^2}{5}} - 0.5\, e^{-\frac{(x-x_D+\Delta x_D/5.16)^2}{5}}, \tag{7}$$

$$F_t(t) = e^{ln(0.01)(\frac{t-0.5T_0}{0.5T_0})^2}. \tag{8}$$

Figure 6 shows the format of the disturbance function along streamwise direction and time and its respective spectral content.

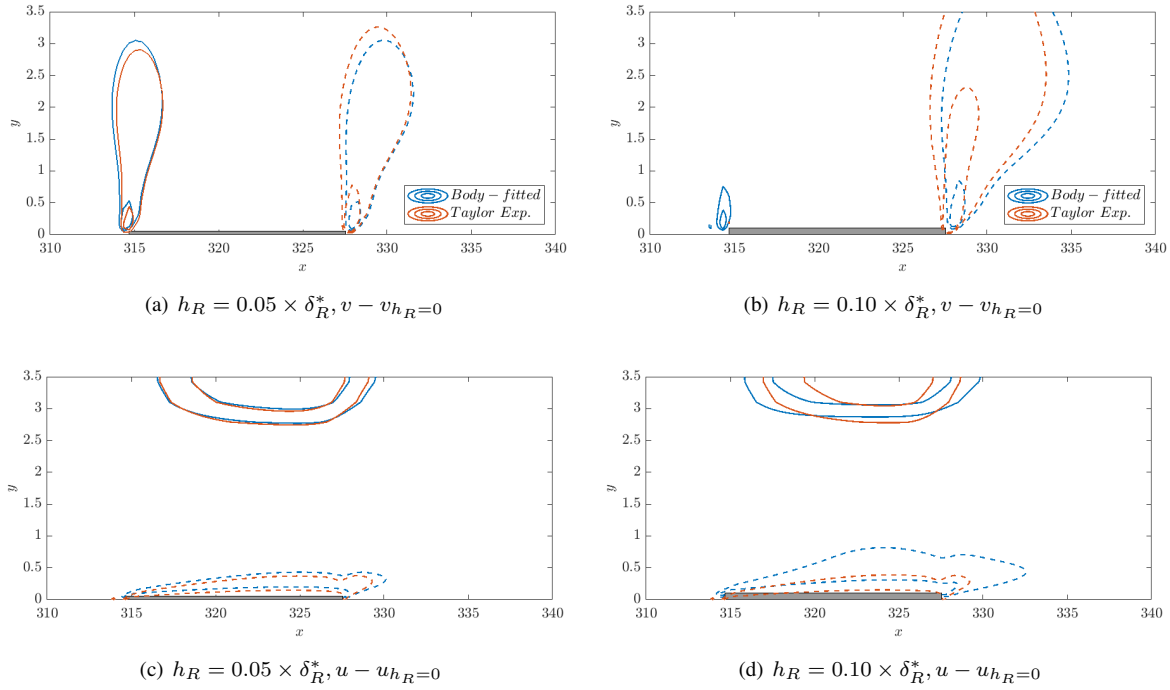

(a) $h_R = 0.05 \times \delta^*_R, v - v_{h_R=0}$ (b) $h_R = 0.10 \times \delta^*_R, v - v_{h_R=0}$

(c) $h_R = 0.05 \times \delta^*_R, u - u_{h_R=0}$ (d) $h_R = 0.10 \times \delta^*_R, u - u_{h_R=0}$

Figure 5. Meanflow distortion caused by the roughness presence for both methods where the levels correspond to 50 and 75% of minimum and maximum values relative to the body-fitted case. (-) positive and (–) negative levels.

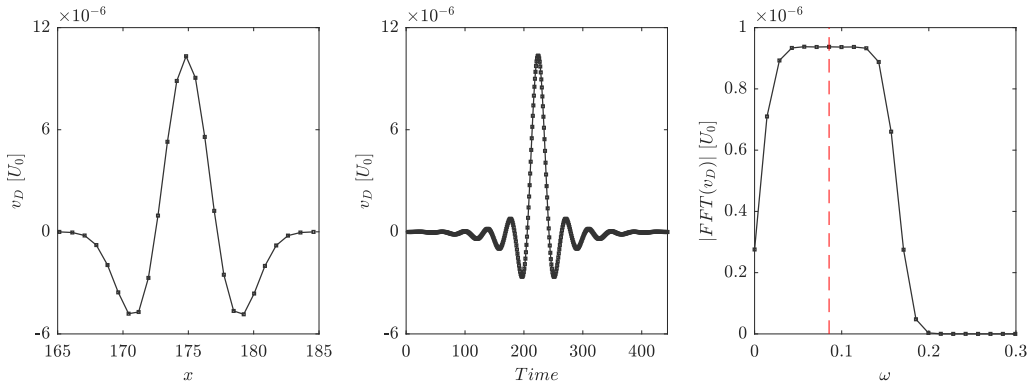

Figure 6. Wave packet disturbance applied at the vertical velocity component at wall and centered at $x_D = 174.83$. Dashed line indicates the central frequency of $\omega = 8.55 \times 10^{-2}$ ($F = 90 \times 10^{-6}$).

For analysis of the disturbance evolution, only the case with smaller roughness, $h_R = 0.05 \times \delta^*_R$, is presented. Another case considering the velocity profiles distortion caused by the disturbance traveling over the roughness region was also simulated. Figure 7 shows the boundary condition obtained considering this correction. As expected, this procedure generated another packet with same wave format of the included packet.

Results of these simulations are presented in Fig. 8, which presents the evolution of the streamwise velocity fluctuation and its relative spectral content at the same points along streamwise stations ($\Delta x = x - x_R$) at $y = 0.4 \times \delta^*$. Results show that the approximation done via Taylor expansion presents reasonable agreement with the body-fitted method but some discrepancies are observed in the spectra amplitude and phase.

Since the roughness height considered the lesser critical case, $h_R = 0.05 \times \delta^*_R$, a better agreement was expected. Preliminary investigations of the possible causes of such discrepancies are discussed. The traditional approximated method could not represent fully the nearfield of a roughness with sharp corners, then the geometry mimicked would be similar to bubble as the streamlines indicate Fig. 4. This seems to be reasonable when observing results of a bidimensional study of roughness with sharp and smoothed corners roughnesses [19]. When

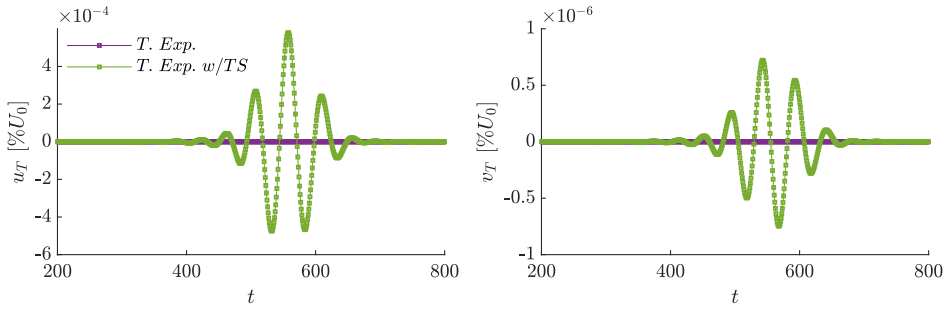

Figure 7. Correction of the boundary condition calculated via approximated method considering the distortion caused by the traveling packet disturbance. Roughness with $h_R = 0.05 \times \delta^*_R$. The amplitudes of case without correction are subtracted.

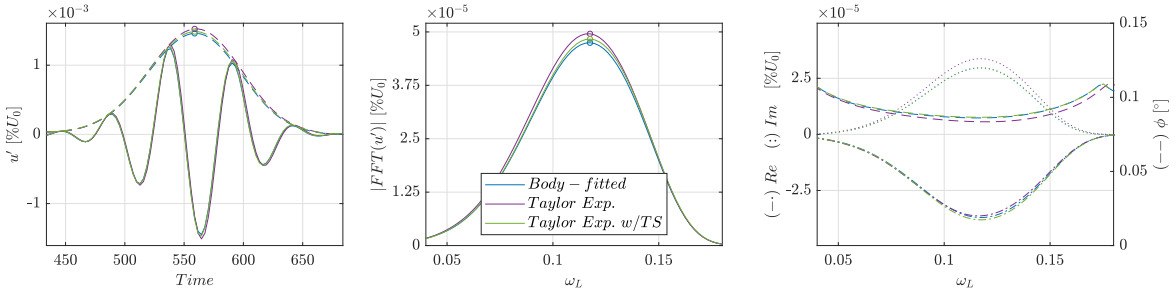

(a) $\Delta x = 0$

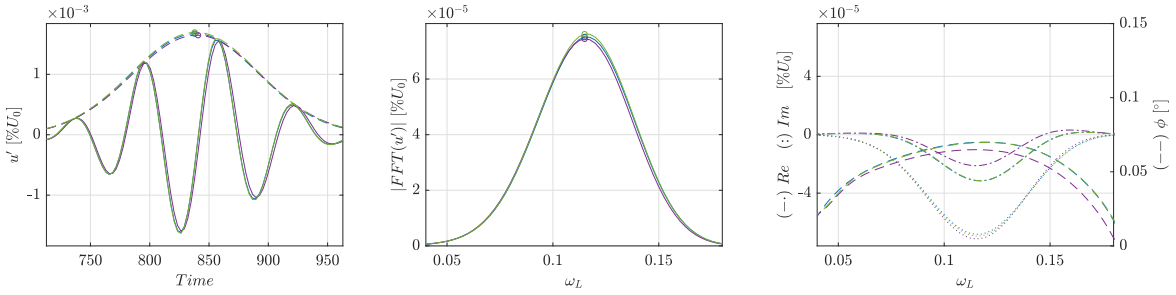

(b) $\Delta x = 65\ mm$

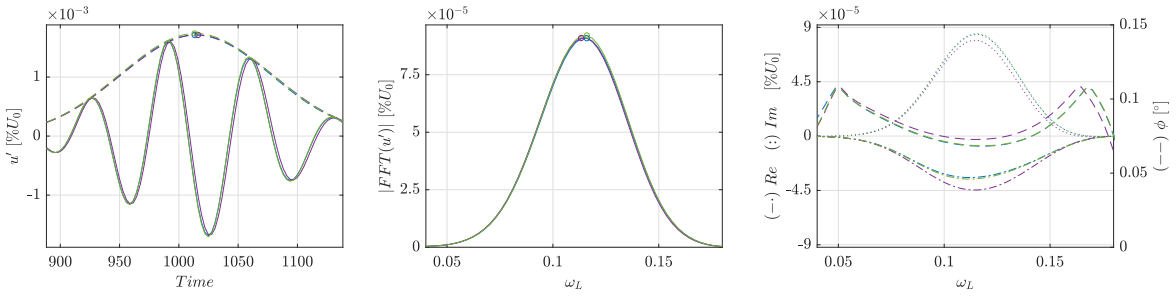

(c) $\Delta x = 105\ mm$

Figure 8. Wavepacket disturbance evolution along the flat plate. First column: (–) streamwise velocity signal and its envelope with maximum value indicated by a (○). Second column: amplitude of signal and its maximum value (○). Third column: real and imaginary parts of the spectra as well as the phase.

the disturbance reach this region, the bubble would also oscillate and cause a phase shift and amplitude difference observed. The T-S wave corrected case would compensate these effects but some other phenomenon related to Stokes layer problem might occurs, since the boundary condition information does not propagate instantaneously to the position of the top surface of the mimicked roughness. Then it adds energy instead of compensating the T-S amplitude at the right moment. Some correction of this delay would provide a better result for this approach.

Acknowledgements. F.H.T.H and M.S.M. are sponsored by Sao Paulo Research Foundation (FAPESP/Brazil) grant #2018/02542-9 and #2018/04584-0, respectively. M.A.F.M. is sponsored by National Council for Scientific and Technological Development (CNPq/Brazil), grant no. 307956/2019-9. Research carried out using the computational resources of the Center for Mathematical Sciences Applied to Industry (CeMEAI) funded by Sao Paulo Research Foundation (FAPESP/Brazil), grant #2013/07375-0, access provided by Prof. José Alberto Cuminato; and resources of the *Barkla* cluster from *High Performance Computing* at Liverpool University, access provided by Prof. Vassilios Theofilis. We would like to thank the US Air Force Office of Scientific Research (AFOSR), grant #FA9550-18-1-0112, managed by Dr. Geoff Andersen from SOARD (Southern Office of Aerospace Research and Development).

Authorship statement. The authors hereby confirm that they are the sole liable persons responsible for the authorship of this work, and that all material that has been herein included as part of the present paper is either the property (and authorship) of the authors, or has the permission of the owners to be included here.

References

[1] Marec, J. P., 2001. Drag Reduction: a Major Task for Research. In Thiede, P., ed, *Aerodynamic Drag Reduction Technologies Proceedings of the CEAS/DragNet European Drag Reduction Conference*, pp. 17–27. Springer, Potsdam, Germany.
[2] Morkovin, M. V., 1969. On the many faces of transition. In *Viscous drag reduction*, pp. 1–31. Springer.
[3] Saric, W. S., Reed, H. L., & Kerschen, E. J., 2002. Boundary-Layer Receptivity to Freestream Disturbances. *Annual Review of Fluid Mechanics*, vol. 34, n. 1, pp. 291–319.
[4] de Paula, I., Würz, W., Mendonça, M., & Medeiros, M., 2017. Interaction of instability waves and a three-dimensional roughness element in a boundary layer. *Journal of Fluid Mechanics*, vol. 824, pp. 624.
[5] Tempelmann, D., Schrader, L.-U., Hanifi, A., Brandt, L., & Henningson, D. S., 2012. Swept wing boundary-layer receptivity to localized surface roughness. *Journal of Fluid Mechanics*, vol. 711, pp. 516–544.
[6] Collis, S. S. & Lele, S. K., 1999. Receptivity to surface roughness near a swept leading edge. *Journal of Fluid Mechanics*, vol. 380, pp. 141–168.
[7] Schrader, L.-U., Brandt, L., & Henningson, D. S., 2009. Receptivity mechanisms in three-dimensional boundary-layer flows. *Journal of Fluid Mechanics*, vol. 618, n. 1, pp. 209–241.
[8] Schrader, L.-U., Amin, S., & Brandt, L., 2010. Transition to turbulence in the boundary layer over a smooth and rough swept plate exposed to free-stream turbulence. *Journal of fluid mechanics*, vol. 646, pp. 297.
[9] Raposo, H., Mughal, S., & Ashworth, R., 2018. Acoustic receptivity and transition modeling of tollmien-schlichting disturbances induced by distributed surface roughness. *Physics of Fluids*, vol. 30, n. 4, pp. 044105.
[10] Raposo, H., Mughal, S., & Ashworth, R., 2019. An adjoint compressible linearised navier–stokes approach to model generation of tollmien–schlichting waves by sound. *Journal of Fluid Mechanics*, vol. 877, pp. 105–129.
[11] Lele, S. K., 1992. Compact finite difference schemes with spectral-like resolution. *Journal of computational physics*, vol. 103, n. 1, pp. 16–42.
[12] Li, N. & Laizet, S., 2010. 2DECOMP & FFT-A Highly Scalable 2D Decomposition Library and FFT Interface. *Cray User Group 2010 conference*, vol. , pp. 1–13.
[13] Bergamo, L. F., Gennaro, E. M., Theofilis, V., & Medeiros, M. A., 2015. Compressible modes in a square lid-driven cavity. *Aerospace Science and Technology*, vol. 44, pp. 125–134.
[14] Martínez, A. G., Gennaro, E. M., & Medeiros, M. A., 2015. Wavepackets in boundary layers close to transonic speeds. *Procedia IUTAM*, vol. 14, pp. 374–380.
[15] Martinez, A. G. & Medeiros, M. A., 2016. Direct numerical simulation of a wavepacket in a boundary layer at mach 0.9. In *46th AIAA Fluid Dynamics Conference*, pp. 3195.
[16] Martinez, A., 2016. *Towards natural transition in compressible boundary layers*. Phd. thesis, University of São Paulo.
[17] Mathias, M. S., 2017. *Instability analysis of compressible flows over open cavities by a Jacobian-free numerical method*. Master thesis, Universidade de São Paulo, São Carlos.
[18] Mathias, M. S. & Medeiros, M., 2018. Direct numerical simulation of a compressible flow and matrix-free analysis of its instabilities over an open cavity. *Journal of Aerospace Technology and Management*, vol. 10.
[19] Franco Sumariva, J. A., Hein, S., & Valero, E., 2020. On the influence of two-dimensional hump roughness on laminar-turbulent transition. *Physics of Fluids*, vol. 32, n. 3, pp. 034102.